RSC Advances

ARTICLE

Precise control of Cu_2O nanostructures and LED-assisted photocatalysis

Received 00th January 20xx,
Accepted 00th January 20xx

DOI: 10.1039/x0xx00000x

www.rsc.org/

Yang Su[a], Arokia Nathan*[a], Hanbin Ma[a], and Hua Wang[b]

We describe the synthesis and characterization of a high-efficiency visible light Cu_2O photocatalyst. Uniform cubic, octahedral and rhombic dodecahedral Cu_2O nanocrystals with a size of 300-600 nm were synthesized using a simple hydrothermal method. Photocatalytic experiments performed for different water samples (a methyl orange solution, toluene solution and industrial wastewater) demonstrate that the rhombic dodecahedral Cu_2O nanocrystals were highly active when driven by low-power white LEDs as a light source. In comparison with other reported photocatalysts, the Cu_2O nanocrystals reported here show a much higher reaction rate and lower electrical energy per order. The reaction rate and photoefficiency were found to be highly correlated with the irradiated photon flux, and the Cu_2O nanocrystals displayed high efficiency in the degradation of aromatic organics. The Cu_2O photocatalyst in this work has the potential to be a low-cost and high-efficiency green technology for wastewater treatment.

Introduction

Visible light photocatalysts with a narrow bandgap could potentially serve as a clean and low-cost strategy for wastewater treatment. Various experiments regarding visible-light photocatalyst materials and the degradation of different categories of organics have been reported[1–4]. Cuprous oxide (Cu_2O), a p-type semiconductor with a direct bandgap of 2.0-2.2 eV, exhibits potential for applications in solar energy conversion[5], hydrogen production[6], gas sensors[7] and organic contamination degradation[8] under visible light. Organic contamination degradation using Cu_2O photocatalysts is demonstrated to have the advantages of high efficiency, low toxicity, good environmental acceptability and low cost[9], making it a promising green technology for wastewater treatment. In past decades, Cu_2O nanocrystals with various structures and their corresponding characteristics have been studied[8,10,11], and the morphology-dependent photocatalytic activity has become a hot topic. Cu_2O {110} facets are reported to show better photocatalytic activity compared to {100} and {111} facets due to their higher density of surface copper dangling bonds[12]. Among photocatalytic reactors, slurry photocatalytic reactors are known to have higher total irradiated surface area per unit volume of photocatalysts and thus a higher reaction rate than that of the immobilized counterparts. Alternately, photocatalyst nanocrystals of smaller size are frequently employed to achieve a higher surface-to-volume ratio and more active sites. A separation process for the recovery of post-treatment photocatalyst particles is necessary for slurry photocatalytic reactors. But the separation of photocatalyst particles with a size of only a few nanometres is not economical. Therefore, high-efficiency photocatalysts with a particle size of a few hundred nanometres are more acceptable. The light source is an important factor for the photocatalytic process. While high power and intensity (hundreds of watts) are frequently engaged in photocatalytic experiments[8,13], very little work has been reported on photocatalytic activity under low-intensity visible light sources[14].

In this work, uniform cubic, octahedral and rhombic dodecahedral Cu_2O nanocrystals with a size of 300-600 nm and pure facets have been successfully prepared using a simple hydrothermal method. Rhombic dodecahedral Cu_2O photocatalysts with all {110} facets exhibit a high reaction rate towards the degradation of methyl orange (MO) driven by low-power white LEDs. The Cu_2O photocatalysts in this work are demonstrated to have a reaction rate that is more than ten times higher and electrical energy per order that is less than one-eighth that of other published reports. The selectivity towards various categories of organics was tested using industrial wastewater. The reaction mechanism was identified with a toluene solution. To the best of our knowledge, this is the first experiment where the as-prepared Cu_2O photocatalysts are found to display capabilities of initiating the ring-opening reactions of aromatic organics and degrading a wide range of organic contaminants effectively.

Results and discussion

[a] Department of Engineering, University of Cambridge, Cambridge CB3 0FA, UK.
[b] Jiangsu Province Environment Monitoring Centre, Nanjing 210036, China.

Electronic Supplementary Information (ESI) available: This includes the scheme of morphology revolution, SEM images, UV-vis spectra, XPS spectra of Cu_2O nanocrystals, cross section of reactor, degradation of MO with 500-nm filter, SEM images of Cu_2O after 5 degradation cycles, and surface atomic arrangement of facet, degradation of toluene. See DOI: 10.1039/x0xx00000x

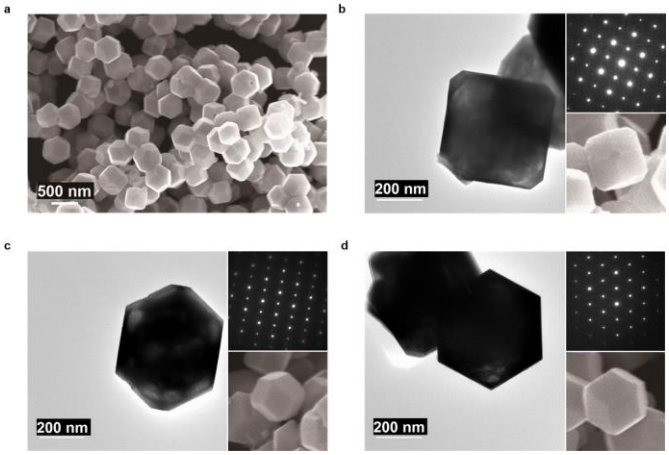

Fig.1 Structure of rhombic dodecahedral Cu_2O nanocrystals: (a) SEM image of Cu_2O nanocrystals. TEM images, SAED patterns and magnified SEM images of Cu_2O nanocrystals viewed along the (b) [100], (c) [110] and (d) [111] directions.

Cu_2O nanocrystals with various morphologies have been successfully prepared using a simple hydrothermal method and the structures can be precisely controlled by adjusting the molar ratio 'r' of hydroxylamine hydrochloride and copper salt as demonstrated in Fig.S1. Cubic structure is formed when r is 8.5, octahedral structure is formed when r increases to 20 while rhombic dodecahedral can be obtained when r reaches 50. The morphologies of as-obtained samples were studied using scanning electron microscopy (SEM) and transmission electron microscopy (TEM). Uniform cubic, octahedral and rhombic dodecahedral Cu_2O nanocrystals with a size of 300-600 nm have been synthesized as demonstrated in Fig.S2 and Fig.1a. Fig.1 also presents the TEM images, the corresponding selective area electron diffraction (SAED) patterns and the magnified SEM images of the as-prepared rhombic dodecahedral Cu_2O nanocrystals viewed along the [100], [110] and [111] directions. It is verified that each cubic Cu_2O nanocrystal has six square {100} facets, each octahedral Cu_2O nanocrystal has eight triangular {111} facets and each rhombic dodecahedral Cu_2O nanocrystal has twelve hexagonal {110} facets. The high crystal quality of the nanoparticles is confirmed by the clear lattice fringes at the edges in the high-resolution TEM images shown in Fig.S3. The optic properties of the as-prepared Cu_2O nanocrystals were measured using Ultraviolet–visible (UV-vis) absorption spectra. Different absorption peaks are detected for cubic and rhombic dodecahedral Cu_2O nanocrystals and the characteristic light-scattering feature from 500 to 1100 nm due to the large particle sizes is observed as shown in Fig.S4[8]. The spectra of the LED light source and the optic properties of the rhombic dodecahedral Cu_2O nanocrystals in the range from 420 to 480 nm are shown in Fig.2a and Fig.2b. The spectrum of the light source, measured by a spectrometer, peaks at 455 nm with a wide range of visible radiation with no UV component (<400 nm). The absorption peak of the as-prepared rhombic dodecahedral Cu_2O nanocrystals corresponds to the peak wavelength of the light source. The phase and purity of the products were determined by X-ray diffraction (XRD) measurements. XRD patterns of the synthesized Cu_2O nanocrystals with the standard Cu_2O XRD pattern (JCPDS No. 05-0667) are presented in Fig.2c. The two patterns match well, indicating no impurities in the prepared products. The chemical

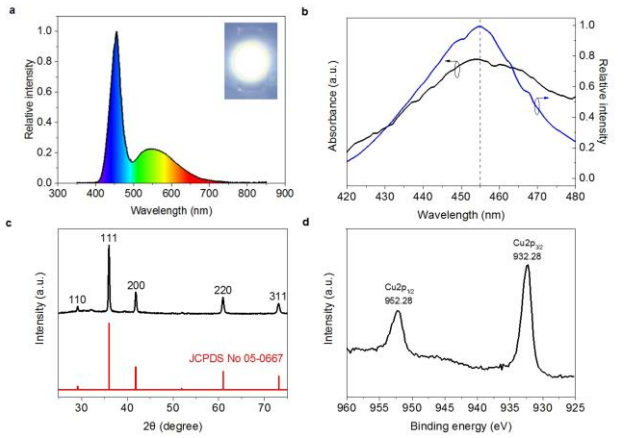

Fig.2 Optical and chemical characterization of Cu_2O nanocrystals: (a) Spectra of LED light sources. Inset: one single LED. (b) UV-vis absorption spectra of rhombic dodecahedral Cu_2O photocatalysts and relative light intensity of LED light sources. (c) XRD pattern. (d) XPS spectrum.

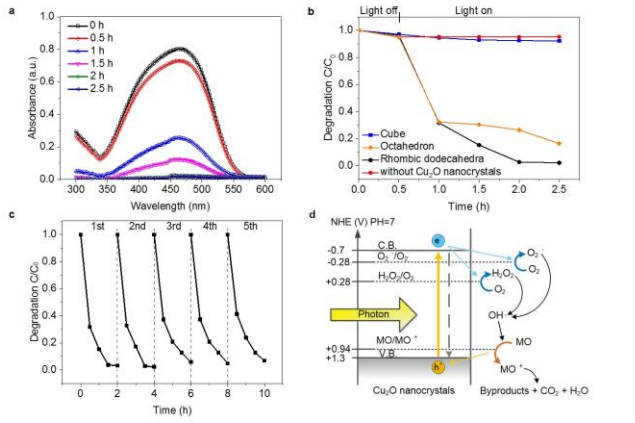

Fig.3 Degradation of MO as a function of irradiation time by 8.880-W LED light sources: (a) Absorption spectra of samples under the degradation of rhombic dodecahedral Cu_2O photocatalysts taken every 30 min. (b) Concentration of MO with and without Cu_2O photocatalysts versus irradiation time. (c) Cycling runs of photocatalytic experiments using rhombic dodecahedral Cu_2O photocatalysts. (d) Possible photocatalysis mechanisms for MO degradation using Cu_2O nanocrystals, C.B. and V.B. denote the conduction and valence bands of Cu_2O nanocrystals, respectively.

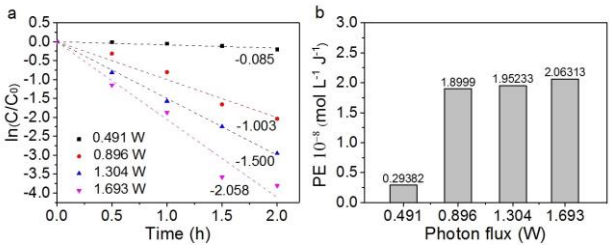

Fig.4 Degradation of MO by rhombic dodecahedral Cu_2O photocatalysts versus irradiation time by LED light sources with different photon flux: (a) Rate constant versus photon flux. (b) Photoefficiency versus photon flux.

composition was studied using characteristic X-ray photoelectron spectroscopy (XPS) as shown in Fig.2d. The XPS peaks of Cu $2p_{1/2}$(952.28 eV) and Cu $2p_{3/2}$ (932.38 eV) are consistent with Copper(I) in Cu_2O nanocrystals[15]. The full XPS spectrum is shown in Fig.S5. No impurities were detected.

The photocatalytic experiments were carried out in a homemade immersion quartz reactor that is reported to have a higher reaction rate than other setups[16] (Fig.S6). Fig.3 presents the degradation of MO versus time using the as-prepared nanocrystals as the photocatalysts under the irradiation of white-light LEDs. The electrical power and the photon flux were measured to be 8.880 W and 1.6929 W, respectively. The absorption spectra of samples under the degradation of rhombic dodecahedral Cu_2O photocatalysts taken every 30 min is displayed in Fig.3a, and the concentrations of the remaining MO are determined by the maximum absorption (λ = 464 nm). The concentrations of MO under the degradation of various Cu_2O photocatalysts and without the photocatalysts are shown in Fig.3b. The remaining concentration of MO keeps almost unchanged for cubic and without Cu_2O photocatalysts. On the contrary, over 83% and over 98% of the MO is degraded by octahedral Cu_2O photocatalysts and rhombic dodecahedral Cu_2O photocatalysts respectively within 2 h under the illumination of low-power visible-light LEDs. The photocatalytic activity stays almost the same for rhombic dodecahedral Cu_2O photocatalysts after five cycling runs of photocatalytic experiments (Fig.3c), indicating its good stability under low irradiance. The excitation wavelength dependency is studied by filtering wavelengths below 500 nm as shown in Fig.S7. The degradation rate of MO using rhombic dodecahedral Cu_2O photocatalysts with the filter is much lower than that without, indicating that the high reaction rate is due to wavelengths below 500 nm. The morphology of rhombic dodecahedral Cu_2O photocatalysts after five cycles of photocatalytic reactions was observed using a SEM as shown in Fig.S8. Some holes and nanosheets can be observed on the surface of the Cu_2O nanocrystals, indicating the {110} facets gradually transform into nanosheets during photocatalytic degradation[9]. The mechanism of the photocatalytic degradation of MO as demonstrated in Fig.3d is proposed as follows: the electrons on the valence band of Cu_2O can be injected into the conduction band when the surface of the Cu_2O nanocrystals is irradiated by visible light (equation (1)). The adsorbed oxygen molecules can be reduced by the electrons on the conduction band to form super oxide radical ions ($O_2^{\cdot-}$, E=-0.28 V) and hydrogen peroxide (H_2O_2, E=+0.28 V), as shown in equations (2) and (3). The excessive $O_2^{\cdot-}$ can further interact with H_2O_2 to generate highly reactive hydroxyl species (OH·) with a redox potential of 1.9 V (equation (4)). The valence band edge level of

Table 1 Photocatalyst performance towards the degradation of MO.

Photocatalyst	m_O (mg)	m_p (g)	t (min)	P (W)	V (ml)	C_0/C_t	R (mg min^{-1} g^{-1})	E_{EO} (kW m^{-3})
Cu_2O (this work)	5.88	0.003	120	8.88	300	50	16.33	34.8
Cu_2O polyhedron[12]	1.2	0.05	180	500	100	5	0.13	$2.15*10^4$
Cu_2O sphere[14]	0.49	0.02	45	32	50	50	0.54	$2.82*10^2$
Cu_2O nanocube[13]	0.67	0.008	120	300	40	6.1	0.70	$1.91*10^4$
Cu_2O/Cu[25]	0.495	0.03	120	40	50	100	0.14	$8.00*10^2$
Cu_2O/ZnO[26]	3.65	0.2	180	200	200	3.7	0.10	$5.28*10^3$
TiO_2/Carbon[27]	81.83	0.5	140	40	200	9.1	1.17	$4.87*10^2$
ZnO/SnO_2[28]	2	0.25	60	300	100	1000	0.13	$1.00*10^3$
$BiVO_4/Pt$[29]	0.3	0.2	900	12	30	1000	0.0017	$2.00*10^3$
Bi_2WO_6/g-C_3N_4[30]	0.5	0.15	180	500	200	1000	0.019	$2.50*10^3$

Cu_2O is estimated to be +1.3 V[17], which is higher than the redox potential of MO (+0.94 V)[18], indicating that MO can be oxidized by both OH· and the holes on the valence band (equations (5) and (6)).

$$Cu_2O + h\nu \rightarrow e^-_{CB} + h^+_{VB} \quad (1)$$

$$(O_2)_{ads} + e^-_{CB} \rightarrow O_2^- \quad E=-0.28\ V \quad (2)$$

$$(O_2)_{ads} + 2H_2O + 2e^-_{CB} \rightarrow H_2O_2 + 2OH^- \quad E=+0.28\ V \quad (3)$$

$$O_2^- + H_2O_2 \rightarrow OH\cdot + OH^- + O_2 \quad (4)$$

$$OH\cdot + MO \rightarrow \text{By-products} + CO_2 + H_2O \quad (5)$$

$$h^+_{VB} + MO \rightarrow \text{By-products} + CO_2 + H_2O \quad (6)$$

The high photocatalytic activity of rhombic dodecahedral Cu_2O photocatalysts towards the degradation of MO can be attributed to two main factors. First, the {110} facets of rhombic dodecahedral Cu_2O nanocrystals with higher surface energy compared to {100} and {111} facets can be easily photoexcited to generate electrons and holes, leading to more active sites[12]. The various photocatalytic activity of {100}, {111} and {110} facets denotes the significance of surface copper dangling bonds. {100} facets with no surface dangling bonds show comparatively low photocatalytic activity. The high density of copper atoms with dangling bonds on the surface of {110} and {111} facets, as demonstrated in Fig.S9, make them positively charged, increasing the concentration of negatively charged MO adsorbed on the surface[19]. {110} facets have higher density of copper dangling bonds compared to {111} facets, leading to higher photocatalytic activity. Second, Cu_2O nanocrystals with oxygen vacancies on the surface are able to adsorb oxygen molecules effectively, which can scavenge electrons to restrain the recombination of electron-hole pairs and generate super oxide radical ions (O_2^-)[20].

To quantitatively evaluate the photocatalytic activity of the as-prepared Cu_2O nanocrystals, the photocatalytic degradation rate can be calculated from equation (7), where R (mg min^{-1} g^{-1}) is the photocatalytic degradation rate, m_o (mg) is the weight of the degraded organic compounds, m_p (mg) is the weight of the photocatalysts used and t (min) is the degradation time. The electrical energy per order (E_{EO}), as an International Union of Pure and Applied Chemistry (IUPAC) standard proposed by Bolton et al.[21], can be utilized to make economic comparisons between various photocatalytic experiments. E_{EO} denotes the power required to reduce the concentration of the contaminant by 1 order of magnitude, where the degradation process obeys the pseudo-first-order kinetics. E_{EO} can be calculated according to equation (8), where P is the electrical power of the light source, t is the degradation time, V is the reactor liquid volume, and C_0 and C_t are the contaminant concentrations before and after photocatalytic degradation, respectively.

$$R = m_o/(m_p * t) \quad (7)$$

$$E_{EO}(kWhm^{-3}\text{-order}) = Pt/(V\log(C_0/C_t)) \quad (8)$$

Various reported photocatalysts and the degradation of MO with their photocatalytic degradation rates and electrical energy per order are listed in Table 1. The rhombic dodecahedral Cu_2O photocatalysts in this work show much higher photocatalytic degradation rates but lower electrical energy per order compared to other works published regarding the degradation of MO, indicating that the synthesized Cu_2O nanocrystals in this work show high photocatalytic activity even under the irradiation of low-power visible light. Photoefficiency and the photocatalytic activity dependency on the photon flux of the light source were carefully studied. The photon flux of four white light LED light sources with different power values was measured using the integrating sphere method and employed for the photocatalytic tests with other

Table 2 Organic category constituents and concentrations before and after the photocatalytic process.

Organic categories	Structure	C(mg/L)
Before photocatalytic process		
Pentadecane		76.3
Dodecane		45.2
Toluene		5.5
Benzen,1,3-dimethyl		7.7
Benzen,1,2,4-trimethyl		8.4
Naphthalene		94.2
Phenol,4-methyl-2-nitro	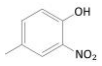	44.7
Naphthalene,2-methyl	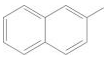	151
Benzocycloheptatriene		73.6
After photocatalytic process		
Pentadecane		5.6
Decanol,2-methyl		0.8
Tetradecane,2,6,10-trimethyl	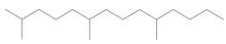	13.9
Tert-hexadecanethiol		8.2
Pentatriacontane, 17-methyl	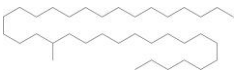	7.6

conditions kept the same. The photocatalytic reactions of all tests obey pseudo-first-order kinetics, and the corresponding first-order rate constants K_{app} are obtained from the linear fit under the condition that the concentrations of organics are of mM scale (equation (9)).

$$\ln(C_t/C_0) = -K_{app}t \quad (9)$$

The first-order rate constants $\mathbf{K_{app}}$ increase from 0.085 h^{-1} for a 0.4910-W photon flux to 2.058 h^{-1} for a 1.6929-W photon flux, as demonstrated in Fig.4a. The initial or overall photoefficiency (PE) can be calculated according to equation (10).

$$PE = r_0/I = K_{app}C_0/I \quad (10)$$

where PE (mol L^{-1} J^{-1}) is the initial or overall photoefficiency, r_0 (mol L^{-1} h^{-1}) is the initial or overall photocatalytic reaction rate and I (W) is the photon flux. The Cu_2O nanocrystals show relatively low overall photoefficiency under the illumination of a 0.491-W photon flux among the four groups of tests as presented in Fig.4b, denoting the insufficiency of the irradiance. The overall photoefficiency increases dramatically when the photon flux reaches 0.896 W. After that, the overall photoefficiency increases slowly with the improvement of the photon flux. It has been reported that under low irradiance, where the photocatalytic reaction is dominant, the photoefficiency remains almost constant. High irradiance leads to the dominance of electron-hole recombination, where photoefficiency shows an inverse square root dependence on irradiance[22]. Therefore, strong light sources should be prevented to achieve economical practical importance. On the other hand, low irradiance is preferable for Cu_2O photocatalysts to weaken photocorrosion and improve stability. The results indicate that the Cu_2O nanocrystals are able to be activated and show a high degradation rate even under low visible photon flux. For low irradiance, a light source with higher photon flux is able to accelerate the photocatalytic reaction but may have limited effects on the overall photoefficiency.

An ideal photocatalyst should be unselective towards the degradation of a wide range of organic compounds. The degradation process of water samples with various organic categories using Cu_2O has not been reported. For the photocatalysis experiment of industrial wastewater, the categories and concentrations of organic compounds before and after 16 hours of degradation by rhombic dodecahedral Cu_2O photocatalysts are shown in Table 2. The water sample was filtered to remove the insoluble substances before treatment and used without dilution. Extremely toxic aromatic compounds are the main pollutants in the solution, and the overall concentration of organics is 506.7 mg/L. After the degradation by Cu_2O photocatalysts, all the aromatic rings are destroyed and the by-products include only linear saturated organic compounds. The overall concentration of organics is reduced to 36.1 mg/L, accounting for 7.12% of the original overall concentration. Toluene solution was used to identify the reaction mechanism. The original concentration of toluene is 2 mg/L and the reaction time is set to be 8 h to ensure the completion of photocatalytic reaction. The concentration of toluene versus the reaction time is shown in Fig.S10. After 6 h of photocatalytic degradation, the remaining toluene concentration is 0.01 mg/L, accounting for 0.5 % of the original concentration. No toluene is detected when the reaction time reaches 8 h. The categories of by-products were recorded using the Thermo Scientific DSQ II GC/MS system. 3-heptanol and 2-methyl-2-propanol were detected during the reaction and no organic compounds were observed after 8 h of photocatalytic reaction. The reaction mechanism is demonstrated in Fig. S10. Cu_2O as a p-type semiconductor with the majority hole carriers is beneficial for the single-electron transform (SET) chemistry with the organic molecules. The ring-opening reaction is initiated by the SET chemistry (i.e., a reaction with holes), whereas OH substitution, ring hydroxylation and alkyl group degradation were induced by hydroxyl-like chemistry[23,24]. The hydroxyl-like chemistry leads to the oxidation/ionization potential drop of aromatic organics, and the SET reactions between the adsorbed contaminants and photocatalysts break the aromatic rings into by-products. The by-products further react with the electrons, holes and hydroxyl species to form smaller molecules and finally carbon dioxide and water. The electrons with high energy level are able to reduce the by-products effectively, leading to the formation of linear saturated molecules. The –SH group of tert-hexadecanethiol is generated from S^{2-} after the photocatalytic reactions, which is ubiquitous in wastewater from oil companies. The concentration of S^{2-} in the wastewater before treatment was measured to be 0.016 mg/L. The remaining long-chain organics result from the electrophilic or nucleophilic reactions of the positively or negatively charged intermediate products.

Conclusions

Uniform Cu_2O nanocrystals with 300-600-nm cubic, octahedral and rhombic dodecahedral morphologies have been synthesized using a simple hydrothermal method. The morphologies can be precisely controlled by adjusting the molar ratio of hydroxylamine hydrochloride and copper salt. The as-prepared rhombic dodecahedral Cu_2O photocatalysts with an optical absorption peak at 455 nm demonstrate high efficiency in degrading MO under the irradiation of low-power visible LED light sources. In our work, the as-prepared Cu_2O nanocrystals with rhombic dodecahedral structure show a reaction rate that is more than ten times higher than and with electrical energy per order that is less than one-eighth that of other published works. Higher photon flux is able to accelerate the photocatalytic process but may have limited impact on the overall photoefficiency under low irradiance. This work demonstrates the ability to degrade aromatic organics and the nature of p-type Cu_2O contribution to the efficient ring-opening reactions of aromatic organics. The Cu_2O photocatalysts in this work may serve as a high-efficiency and low-cost green technology for wastewater treatment.

Experimental section

Materials

Copper(II) chloride (97%), hydroxylamine hydrochloride (99%), SDS (98.5%) and methyl orange (100%) were purchased from Sigma Aldrich. Sodium hydroxide (98%) was purchased from Fisher brand. All chemicals were used as received without further purification.

Synthesis of Cu_2O nanocrystals

Cu_2O nanocrystals were synthesized using a simple hydrothermal method. 67 mg $CuCl_2$ and 1 g SDS were dispersed in 65 mL deionized water. The solution was placed in a water bath set at 35 ˚C with vigorous stirring for 10 min. 10 mL of 0.2 M NaOH was introduced. 25 mL of 0.17 M, 0.4 M and 1.0 M $NH_2OH{\cdot}HCl$ was added to three samples, respectively. The solution was stirred for 30 s and kept in the water bath for 1 h. The products were centrifuged at 5000 rpm for 4 min, and the precipitate was washed and centrifuged twice using 50 mL of water and ethanol. The obtained product was dried in the oven at 60 ˚C for 12 h.

Nanocrystal characterization

The morphologies of synthesized nanocrystals were studied using LEO GEMINI 1530VP scanning electron microscopy (SEM) at 8 KV and FEI Tecnai G² 20 transmission electron microscopy (TEM) at 200 kV. Ultraviolet–visible (UV-vis) absorption spectra was recorded using a UniCam UV/VIS spectrometer v.2. X-ray diffraction (XRD) patterns were obtained by a BRUKER D8 ADVANCE diffractometer with Cu Kα radiation. X-ray photoelectron spectroscopy (XPS) measurements were performed using a PHI5000VersaProbe II scanning XPS microscope. The structure and atomic arrangement of Cu_2O nanocrystals were drawn using Material Studio.

Photocatalysis experiment

White light LEDs were used as the light source. The spectra of the light source were measured using a Labsphere CDS-600 spectrometer. The power and photon flux were measured using a EVERFINE PMS-80 integrating sphere. The photocatalysis experiment on the degradation of MO was carried out in a homemade quartz immersion reactor with a volume of 330 mL at room temperature. 3 mg of Cu_2O photocatalysts were dispersed in 300 mL of 20 mg/L MO solution. The solution was constantly stirred in the dark for 15 min to reach the adsorption and desorption equilibrium. 1.5 mL of the solution was sampled every 30 min and centrifuged at 5000 rpm for 4 min to separate the photocatalysts from the solution. The UV-vis absorption spectra of the samples was recorded. The industrial wastewater was collected from an oil company and 3 mg photocatalysts and 60 mL solution were used. The solution was filtered and the PH value was adjusted to 7 before the test, and the photocatalysis experiment was carried out in a 100-mL quartz immersion reactor irradiated by the LED light source with vigorous magnetic stirring. For the degradation of toluene solution, 3 mg photocatalysts were dispersed in 300 mL, 2 mg/L toluene solution. The photocatalytic reaction was carried out in a 330 mL reactor under LED illumination and with vigorous magnetic stirring. The categories and concentrations of organic compounds were studied using a Thermo Scientific DSQ II GC/MS system.

Notes and references

1 J. Li, S. K. Cushing, J. Bright, F. Meng, T. R. Senty, P. Zheng, A. D. Bristow and N. Wu, *ACS Catal.*, 2013, **3**, 47–51.

2 T. Zhu, W. Li Ong, L. Zhu and G. Wei Ho, *Sci. Rep.*, 2015, **5**, 10601.

3 S. Ghosh, N. a Kouamé, L. Ramos, S. Remita, A. Dazzi, A. Deniset-Besseau, P. Beaunier, F. Goubard, P.-H. Aubert and H. Remita, *Nat. Mater.*, 2015, **14**, 505–11.

4 L. Zhu, M. Hong and G. Wei Ho, *Sci. Rep.*, 2015, **5**, 11609.

5 R. N. Briskman, *Sol. Energy Mater. Sol. Cells*, 1992, **27**, 361–368.

6 M. Hara, T. Kondo, M. Komoda, S. Ikeda, J. N. Kondo, K. Domen, M. Hara, K. Shinohara and A. Tanaka, *Chem. Commun.*, 1998, **2**, 357–358.

7 J. Zhang, J. Liu, Q. Peng, X. Wang and Y. Li, *Chem. Mater.*, 2006, **18**, 867–871.

8 W. C. Huang, L. M. Lyu, Y. C. Yang and M. H. Huang, *J. Am. Chem. Soc.*, 2012, **134**, 1261–1267.

9 Z. Zheng, B. Huang, Z. Wang, M. Guo, X. Qin, X. Zhang, P. Wang and Y. Dai, *J. Phys. Chem. C*, 2009, **113**, 14448–14453.

10 H. Xu, W. Wang and W. Zhu, *J. Phys. Chem. B*, 2006, **110**, 13829–13834.

11 C. H. Kuo, C. H. Chen and M. H. Huang, *Adv. Funct. Mater.*, 2007, **17**, 3773–3780.

12 X. F. L. In, R. M. Z. Hou, J. Q. Z. Hang and X. H. S. Heng, 2010, **28**, 5073–5079.

13 W. Sun, W. Sun, Y. Zhuo and Y. Chu, *J. Solid State Chem.*, 2011, **184**, 1638–1643.

14 Y. Wang, D. Huang, X. Zhu, Y. Ma, H. Geng, Y. Wang, G. Yin and D. He, *Nanoscale Res. Lett.* 2014, 36–38.

15 M. Wang, L. Sun, Z. Lin, J. Cai, K. Xie and C. Lin, *Energy Environ. Sci.*, 2013, **6**, 1211–1220.

16 H. De Lasa, *Photocatalytic Reaction Engineering*, 2005.

17 A. Paracchino, V. Laporte, K. Sivula, M. Grätzel and E. Thimsen, *Nat. Mater.*, 2011, **10**, 456–461.

18 T. Kou, C. Jin, C. Zhang, J. Sun and Z. Zhang, *RSC Adv.*, 2012, 12636–12643.

19 J. Y. Ho and M. H. Huang, *J. Phys. Chem. C*, 2009, **113**, 14159–14164.

20 M. Hara, T. Kondo, M. Komoda, S. Ikeda, K. Shinohara, A. Tanaka, J. N. Kondo, K. Domen, M. Hara, K. Shinohara and A. Tanaka, *Chem. Commun.*, 1998, **2**, 357–358.

21 J. R. Bolton, K. G. Bircher, W. Tumas and C. a. Tolman, *Pure Appl. Chem.*, 2001, **73**, 627–637.

22 D. F. Ollis and N. Serpone, *Environ. Sci. Technol.*, 1991, **25**, 1522–1529.

23 X. Li, J. W. Cubbage, T. a. Tetzlaff and W. S. Jenks, *J. Org. Chem.*, 1999, **64**, 8509–8524.

24 X. Li, J. W. Cubbage and W. S. Jenks, 1999, 8525–8536.

25 B. Zhou, Z. Liu, H. Wang, Y. Yang and W. Su, *Catal. Letters*, 2009, **132**, 75–80.

26 C. Xu, L. Cao, G. Su, W. Liu, H. Liu, Y. Yu and X. Qu, *J. Hazard. Mater.*, 2010, **176**, 807–813.

27 Y. Li, X. Li, J. Li and J. Yin, *Water Res.*, 2006, **40**, 1119–1126.

28 C. Wang, X. Wang, B.-Q. Xu, J. Zhao, B. Mai, P. Peng, G. Sheng and J. Fu, *J. Photochem. Photobiol. A Chem.*, 2004, **168**, 47–52.

29 L. Ge, *J. Mol. Catal. A Chem.*, 2008, **282**, 62–66.

30 L. Ge, C. Han and J. Liu, *Appl. Catal. B Environ.*, 2011, **108-109**, 100–107.